Journal of Biomedical Optics

SPIEDigitalLibrary.org/jbo

Hydrophobic cyanine dye-doped micelles for optical *in vivo* imaging of plasma leakage and vascular disruption

Bálint Botz
Kata Bölcskei
Ágnes Kemény
Zoltán Sándor
Valéria Tékus
György Sétáló, Jr
Janka Csepregi
Attila Mócsai
Erika Pintér
László Kollár
Zsuzsanna Helyes

SPIE

Journal of Biomedical Optics 20(1), 016022 (January 2015)

Hydrophobic cyanine dye-doped micelles for optical *in vivo* imaging of plasma leakage and vascular disruption

Bálint Botz,[a,b,*] Kata Bölcskei,[a,b] Ágnes Kemény,[a,b] Zoltán Sándor,[a] Valéria Tékus,[a,b] György Sétáló Jr,[c,d] Janka Csepregi,[e] Attila Mócsai,[e] Erika Pintér,[a,b] László Kollár,[f] and Zsuzsanna Helyes[a,b,g]

[a]University of Pécs, School of Medicine, Department of Pharmacology and Pharmacotherapy, Szigeti út 12, Pécs H-7624, Hungary
[b]University of Pécs, János Szentágothai Research Centre, Molecular Pharmacology Research Team, Ifjúság útja 20, Pécs H-7624, Hungary
[c]University of Pécs, School of Medicine, Department of Medical Biology, Szigeti út 12, Pécs H-7624, Hungary
[d]University of Pécs, János Szentágothai Research Centre, Signal Transduction Research Team, Ifjúság útja 20, Pécs H-7624, Hungary
[e]Semmelweis University School of Medicine and MTA-SE "Lendület" Inflammation Physiology Research Group, Department of Physiology, Tűzoltó u. 37-47, Budapest H-1094, Hungary
[f]University of Pécs, Department of Inorganic Chemistry, Ifjúság útja. 6, Pécs H-7624, Hungary
[g]MTA-PTE NAP B Pain Research Group, Szigeti út 12., Pécs H-7624, Hungary

Abstract. Vascular leakage is an important feature of various disease conditions. *In vivo* optical imaging provides a great opportunity for the evaluation of this phenomenon. In the present study, we focus on the development and validation of a near-infrared (NIR) imaging formula to allow reliable, cost-efficient evaluation of vascular leakage in diverse species using the existing small-animal fluorescence imaging technology. IR-676, a moderately hydrophobic NIR cyanine dye, was doped into self-assembling aqueous micelles using a widely employed and safe nonionic emulsifier (Kolliphor HS 15), and was tested in several acute and chronic inflammatory disease models in both mice and rats. The imaging formula is stable and exerts no acute toxic effects *in vitro*. It accumulated specifically in the inflamed regions in all models, which could be demonstrated by both conventional epifluorescence imaging, and fluorescence tomography both as a standalone technique and also by merging it with computed tomography scans. *Ex vivo* verification of dye accumulation by confocal fluorescence microscopy was also possible. The present formula allows sensitive and specific detection of inflammatory plasma leakage in diverse models. Its potential for imaging larger animals was also demonstrated. IR-676-doped micelles offer an excellent opportunity to image inflammatory vascular leakage in various models and species. [DOI: 10.1117/1.JBO.20.1.016022]

Keywords: animal model; inflammation; plasma leakage; fluorescence; micelle; optical imaging; fluorescence tomography.

Paper 140600RR received Sep. 21, 2014; accepted for publication Dec. 30, 2014; published online Jan. 28, 2015.

1 Introduction

The interest in near-infrared (NIR) optical *in vivo* imaging is constantly growing since its debut in the early 2000s,[1] and the sensitivity and versatility of the instruments have increased considerably since then. However, there is only a narrow range of reliable contrast agents currently available, and this is especially true for fluorescence markers dedicated to image plasma leakage from diseased vasculature. Most of these probes either suffer from low contrast and signal-to-background ratio, or have tremendous operational costs, thereby limiting large-scale imaging, and in general, do not enable studies involving research animals larger than mice.

The dilation and increased permeability of the microvessels caused by the contraction of the endothelial cells in the area of inflammation and subsequent formation of intercellular gaps is an important adaptive change during acute vascular hyperpermeability, as this helps the transmigration of immune cells (e.g., leukocytes, T, and B cells) as well as the transport of antibodies and inflammatory mediators to the site of the disease.[2] Prolonged tissue ischemia and the following reperfusion leads to a similarly increased perfusion and permeability of the vasculature within the affected area. This process leads to the formation of a plasma protein-rich fluid exudate as well, thereby contributing to edema formation, a characteristic feature of acute inflammation. This takes place primarily in the postcapillary venules.[3] Chronic vascular hyperpermeability (CVH) is mainly observed in tumors and chronic inflammatory conditions such as rheumatoid arthritis or immune-mediated dermatitis. The main difference of CVH is that the plasma leakage occurs primarily from newly formed pathological, "leaky" vessels with weakened endothelial structures.[3]

It is not surprising that noninvasive, longitudinal, real-time evaluation of these processes provides a great opportunity to estimate the extent and characteristics of these conditions, for which NIR optical imaging is an excellent alternative in preclinical settings compared to other modalities (computed tomography etc.) due to the availability of tabletop instruments and lack of ionizing radiation.[4]

The underlying principle of optical *in vivo* imaging of this phenomenon is based on employing NIR fluorophores (emission maximum between 650 and 900 nm), whose particle size is great enough to limit their escaping from healthy vasculature under normal conditions; however, they retain their ability to

*Address all correspondence to: Balint Botz, E-mail: balint.botz@gmail.com

leave leaky vessels of inflamed or tumor tissues. The earliest example was the Evans-blue method (Miles-assay), which relied on the iv. administration of the azo dye with high affinity for serum albumin, for which the degree of extravasation could be traditionally determined by spectrophotometry.[3] It was recently demonstrated though that *ex vivo* NIR imaging of the affected organs is superior in terms of both specificity and sensitivity,[5] and *in vivo* fluorescence imaging of this dye is also feasible.[6] Unfortunately, this technique gives meaningful results only with a very high amount of concentrated dye, which necessitates the sacrificing of the subject, and can be easily biased if the residual dye in the vasculature is not properly removed. Consequently several authors employed other, mainly cyanine fluorophores such as indocyanine green (ICG), Cy5.5, or IR-820 which also have nonspecific binding ability to albumin and other plasma proteins.[7–10] The signal strength and contrast of these techniques remained relatively modest despite the high doses administered, presumably due to aspecific binding, small size, and the short plasma half-life (typically only minutes) of these compounds regardless of plasma protein binding (as the parenchymal cells of the liver rapidly clear these substances from the circulation). However, these studies substantiated that (1) cyanine dyes are, in general safe, and can be used for noninvasive tracking of plasma extravasation and (2) the signal intensity of extravasated dye is relatively stable, mainly due to nonspecific uptake by phagocytes. Among the dyes currently used, ICG received by far the most attention despite its significant disadvantages compared to novel, advanced cyanine fluorophores (low stability in aqeous media and low quantum yield, small Stokes-shift, autoaggregation, as well as poor solubility in physiologic buffers) as it is currently the only FDA-approved NIR-dye due to historical reasons.[11] Additionally, its cytotoxic effects have also been reported.[12,13] An advanced ICG-derivative SIDAG demonstrated somewhat better sensitivity and lower toxicity than ICG; nevertheless, it still required relatively large doses to be administered and contrast remained negligible at early imaging time points.[14]

To overcome the difficulties outlined above, and to get better results, several investigators prepared preformulated NIR contrast agents that do not rely on plasma protein binding either by (1) performing a controlled labeling of a macromolecule (albumin, dextranes, etc.) *in vitro*, prior to use[15–18] or (2) synthesizing fluorescently labeled microparticles whose extravasating capabilities are limited by their size.[19–21] The latter method could especially provide additional benefits, as the incorporation of the dye into a nanoprobe minimizes the potential cytotoxicity and delays systemic elimination, thereby leading to prolonged plasma half-life. Here, we have employed Kolliphor HS 15 for this purpose, a nonionic solubilizer that forms stable micelles in water and physiologic buffers with an average size of 12 nm, and has a negligible toxicity on its own.[22]

Based on these findings there is a particular need in preclinical inflammation and vascular research to have an NIR contrast agent with the following characteristics: (1) absolute compatibility with both the existing fluorescence molecular tomographic technology and confocal fluorescence microscopy to enable *ex vivo* verification, (2) imaging capability of both superficial and deep-tissue plasma leakage with a broad spectrum of applicability, (3) simple and cost-efficient synthesis requiring only standard life sciences laboratory equipment, and down-to-earth steps during the process, and (4) potential for imaging larger animals (rats etc.). Therefore, we aimed at synthesizing a novel formula to fulfill these criteria and validate it in well established and routinely used rodent inflammation models of different organs.

2 Materials and Methods

2.1 *Preparation of the IR-676-Doped Micelles*

The moderately hydrophobic pentamethine cyanine fluorescent dye IR-676 (1,1′,3,3,3′,3′-hexamethyl-4,5,4′,5′-dibenzoindodicarbocyanine)-iodide [Fig. 1(a)] was selected as a promising candidate, as (1) it has low water solubility (but is still not insoluble), and is moderately soluble in other polar solvents (e.g., lower alcohols) (2) its excitation/emission wavelength maxima differ only marginally from some other widely used "gold standard" NIR fluorophores (Cy5.5, Alexa Fluor 680, etc.), thereby ensuring compatibility with the existing imaging technology and wavelength filters. It has also been previously demonstrated that this dye is an excellent calibration standard for fluorescence tomography systems.[23] IR-676 was obtained in powder form (MW: 610.58 g/mol, excitation maximum: 676 nm, emission maximum: 700 nm, Spectrum-Info Ltd., Kyiv, Ukraine). The dye can be easily dissolved in dichloromethane or alcohols.[23,24] Taking into consideration the incompatibility of dichloromethane with most plastic materials, the dye was initially dissolved in methanol at room temperature (RT), and was ultrasonicated then stirred until it formed a clear, deep blue solution with a concentration of 2×10^{-4} M. This stable stock solution was either immediately used, or stored at −20°C protected from light. 100 μl batches were pipetted into microtubes which were covered with a parafilm membrane pierced by a 27G needle three to four times to allow evaporation of the solvent at a moderate rate. The vials were then centrifuged for at least 60 min in a Speed Vac centrifuge (Savant RVT4104 refrigerated vapor trap, Savant Instruments Inc, Farmingdale, New York), leaving behind a thin film of dried dye at the bottom of the vial, which was stored light protected at 4°C. For the reconstitution, a 5 w/v% solution of the nonionic surfactant Kolliphor HS 15 (Polyethylene glycol-15-hydroxystearate, Sigma-Aldrich) was prepared in sterile deionised water. Kolliphor HS 15 was selected based on its outstanding *in vivo* safety and previously demonstrated effectiveness for imaging contrast agent formulas such as ICG.[22,25–26] 500 μl batches of this medium were directly pipetted into the microtubes containing the dye at RT. Complete dissolution of IR-676 could be achieved within 10 to 20 min by vortexing and ultrasonication. The resulting stable solution (4×10^{-5} M) was either immediately used, or stored at 4°C for a maximum of 48 h.

2.2 *Animals*

For the experiments, 10 to 12-week-old C57Bl/6 mice (weighing 20 to 25 g) and 5-week-old Wistar rats (weighing 125–150 g) were used, for which the original breeding pairs were obtained from Charles-River Hungary Ltd. (Budapest, Hungary). The animals were bred in the Laboratory Animal House of the Department of Pharmacology and Pharmacotherapy at the University of Pécs, fed with standard rodent chow and water *ad libitum*, kept at 24°C to 25°C ambient temperature and 12-h light-dark cycles. The studies were approved by the Ethics Committee on Animal Research of the University of Pécs according to the Ethical Codex of Animal Experiments (license No: BA 02/2000-2/2012 and BA02/2000-5/2011).

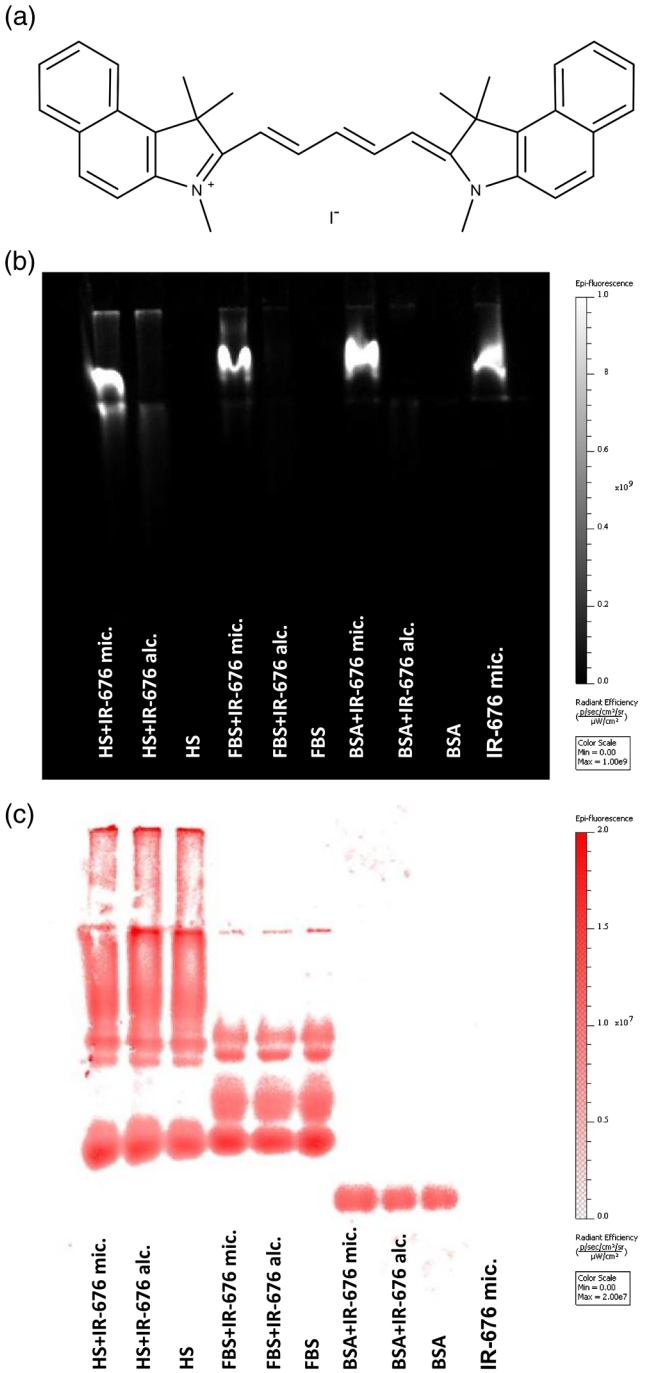

Fig. 1 The structure of IR-676 and the binding ability of the formula to serum proteins. (a) IR-676 displays a pentamethine cyanine backbone structure similarly to other, more common fluorophores (Cy5.5 etc.). As the side chains are single methyl groups, the water-solubility and reactivity of the dye is low. (b) IR-676 fluorescence measurement following native polyacrylamide gel electrophoresis of bovine serum albumin (BSA), fetal bovine serum (FBS), and horse serum (HS) samples incubated with ethanol (20 v/v%) or Kolliphor HS 15 (5 w/v%)-based solutions of IR-676. (c) Fluorescence image of the same gel following protein-staining with Coomassie brilliant blue.

2.3 *Imaging Protocol*

The IR-676-based contrast agent was injected iv. in a dosage of 2×10^{-7} mol/kg body weight, corresponding to a convenient injectate volume of 100 to 150 μl for mice or 0.6 to 0.8 ml for rats. The method of delivery was either lateral tail vein (oxazolone- and carrageenan-model) or retro-orbital injection (in the other models). Imaging was performed at several selected time-points with the *in vivo* imaging system (IVIS) Lumina II (PerkinElmer Ltd., Waltham, Massachusetts) with a 640-nm excitation (535, 570, and 605 for spectral unmixing) and ~700-nm emission filters, auto exposure time, and a binning factor of 2. Fluorescence was expressed as the total radiant efficiency $[(\text{photons/s/cm}^2\text{/steradian})/(\mu\text{W/cm}^2)]$. The fluorescence molecular tomography (FMT) 2000 system (PerkinElmer Ltd.) was calibrated using the instrument's 680-nm laser channel, and a sample solution of 1×10^{-6} M following the instructions of the instrument's manufacturer. Imaging with the FMT system was performed uniformly 3 h postinjection due to the lower throughput of the three-dimensional (3-D) imaging system using high-resolution acquisition parameters. Fluorescence was expressed as either the calculated amount of fluorophore (pmol) or as surface fluorescence (counts/energy). In the airway inflammation model, the extent of the inflamed area was also expressed in μm^3. Animals were anesthetized for the injection and imaging with ketamine-xylazine ip. (dosage: 100:5 mg/kg). During anesthesia, body temperature was maintained by a heating lamp and vital signs were monitored by observation until recovery. Home cage activity after recovery was also observed.

2.4 *Interaction with Serum Proteins*

To determine whether IR-676 binds to serum proteins in its freely dissolved or encapsulated state, ethanol-based (20 v/v %) or micellar (5 w/v%) solutions (10 μl, 4×10^{-5} M) of the dye were incubated with bovine serum albumin (BSA) (0.5 mg/ml), fetal bovine serum (FBS), and horse serum (HS) (10x dilution) samples (100 μl) at RT. Additionally, the encapsulated dye was also incubated in an equal amount of deionised water. 10 μl batches of the samples were mixed with an equal amount of loading dye (bromophenol-blue solution) and 10 μl of the mixtures were pipetted into the gel. To preserve the physiologic protein structure and potential nonspecific binding, samples were separated by nondenaturing polyacrylamide gel electrophoresis (PAGE) (100 V, 1.5 h, Tris/glycine buffer).[27] Gels were scanned using the IVIS Lumina II, then stained with Coomassie brilliant blue and imaged again using the same settings (Note: the fluorescence spectra of the two dyes overlap, and the methanol-based Coomassie-staining procedure removes IR-676 from the gel).

2.5 *In Vitro Toxicity Screening*

The biological safety of the formula was evaluated on the Chinese Hamster Ovary (CHO-K1) cell line. Cells were trypsinized, washed, and resuspended in PBS at a density of 2×10^5/ml. 50 or 100 μl batches of the imaging formula or the vehicle alone were added to 1 ml amounts of cells; thereafter, the cells were incubated for 5 min at 37°C, pelleted by centrifugation at 1000 rpm for 5 min, after which they were resuspended in 1 ml PBS. Cell viability was evaluated by the fluorescein diacetate-propidium iodide (FDA/PI) assay,[28] as 500 μl batches of each sample were stained with either FDA (1 μl of an 500-mM stock solution in dry DMSO) or PI (5 μl of 0.75-mM stock solution) and incubated for 10 min. Viable cells fluoresce in green as they enyzmatically convert FDA to fluorescin, whereas dead cells fluoresce in red as PI stains the nuclei after passing through the damaged cell membranes. 2×10^4 cells/cohort were evaluated by a CyFlow flow cytometer (Partec Ltd., Münster,

Germany). Untreated and 6% formalin fixed cells were used to set the gates for living and dead cells, respectively. The percentages of viable and nonviable cells were calculated by identical gating for each sample.

2.6 *Preparation of the Frozen Ear Sections for Microscopy*

The samples were embedded in a frozen section compound (FSC 22, Surgipath Ltd., Richmond, Illinois), immediately frozen in liquid nitrogen, and stored at −80°C. The samples were cryosectioned (8 μm), and imaged within 24 h by an Olympus FluoView 1000 confocal laser scanning fluorescence microscope (Olympus, Center Valley, Pennsylvania). Single optical sections were taken from areas of interest using a 40× objective.

2.7 *Oxazolone-Induced Contact Dermatitis Mouse Model*

The ear model of oxazolone-induced allergic contact dermatitis was previously validated as a robust, reliable disease model, leading to localized edema and sensitization, as well as inflammatory cell activation primarily mediated by Th1 cell response.[29] Moreover, it has been recently demonstrated as a good proof-of-concept model to test potential NIR tracers of vascular leakage.[30] Anesthetized mice were sensitized on two consecutive days by applying 50 μl 2% oxazolone (Sigma-Aldrich) onto the shaved abdomen. Six days later, 15 − 15 μl of 2% oxazolone was applied on both the inner and outer surfaces of the right ear, whereas the left ear was treated with the vehicle only (96% ethanol) to serve as control. The oxazolone treatment induces a marked hyperemia and edema within hours, accompanied by leukocyte influx and T cell infiltration. Subjects were injected with the contrast agent 24 h later, and were repeatedly imaged between 5 to 180 min postinjection with the IVIS Lumina II. Thereafter, the mice were sacrificed, and ears were collected for cryosection histology.

2.8 *Lipopolysaccharide-Induced Acute Airway Inflammation Mouse Model*

The LPS model is a reliable tool to investigate acute inflammatory changes of the airways and lungs, and has been validated and optimized by our workgroup before.[31] In the present series of experiments, a modified, direct intratracheal delivery was used, since our preliminary experiments demonstrated that the conventionally used intranasal route produces far too high intra-group variations for *in vivo* imaging, Mice were anesthetized, and a PE-10 cannula was carefully introduced into the trachea via the mouth by a novel technique allowing simple visualization of the vocal cords.[32] The airway inflammation was induced by intratracheal instillation of 60 μl PBS in which 100 μg dry, purified Escherichia coli (serotype: 083) endotoxin was dissolved while controls received PBS. 21 h after LPS treatment, the mice were injected with the contrast agent, and they were imaged 3 h later by the FMT 2000 imaging system.

2.9 *K/BxN Serum-Transfer Arthritis Mouse Model*

The K/BxN serum-transfer model is a reliable immune-mediated model of rheumatoid arthritis, which is based on the transfer of autoantibody-rich sera from the spontaneously arthritic K/BxN mice into healthy recipients, thus eliciting a transient polyarthritis. Sera were obtained from the K/BxN mice, pooled, and stored at −80°C as described earlier.[33] To induce a systemic polyarthritis, mice were injected ip. with 300 μl serum diluted to 1 ml with sterile PBS. Subjects were injected 7 days after arthritis induction, and were imaged 3 h postinjection using the FMT 2000 system.

2.10 *Carrageenan-Induced Acute Paw Inflammation Model of the Rat*

This model was selected to evaluate the feasibility of *in vivo* imaging of larger species with this contrast agent. Carrageenan is a complex polysaccharide which elicits a massive edema formation, local hyperemia, and consequent leukocyte accumulation, thus serving as a reliable model of acute inflammation.[34] Wistar rats under anesthesia received an intraplantar injection of 100 μl 1% carrageenan (Sigma-Aldrich) in the left hindpaw, while the right paw was injected with an equal volume of saline. Two hours later, the animals were injected with the contrast agent, and were imaged 60 and 120 min postinjection with the IVIS Lumina II.

2.11 *Statistical Analysis*

Results are expressed as mean ± standard error of the mean. Statistical evaluation was performed by Graphpad Prism®. The imaging results in the oxazolone model were evaluated by two-way ANOVA with Sidak's multiple comparisons test, while other imaging results were achieved by Student's two-tailed *t*-test. At least $p < 0.05$ was considered significant.

3 Results

3.1 *The IR-676-Based Formula Demonstrates Negligible Binding to Serum Proteins*

The nondenaturing-PAGE demonstrated that IR-676 binds weakly if at all to serum proteins regardless of being present as freely dissolved (ethanol) or encapsulated (Kolliphor HS 15). As strong fluorescence was exclusively observed in the wells where micellar IR-676-containing samples were pipetted, which did not propagate in the gel, we can conclude that the formula did not disintegrate even when exposed to strong electric current, and its size prevented it from entering into the gel [Figs. 1(b) and 1(c)].

3.2 *The Dye Formula Has No Impact on Cell Viability in the Fluorescein Diacetate-Propidium Iodide Acute Toxicity Assay*

Exposing CHO-K1-cells to two concentrations of the formula or the vehicle alone exerted no apparent acute toxic effects. The percentage of viable and dead cells showed minimal fluctuations between study groups (Table 1). As the higher concentration employed (100 μl formula/1 ml cell suspension) exceeded even the expected peak plasma concentration upon intravenous injection, we assume that the present formula poses minimal if any risks of toxicity within its suggested operational range.

Although no formal *in vivo* toxicity tests were performed, we carefully observed IR-676-treated animals to assess any major untoward effect. No lethality occurred throughout the study and no observable pathological sign was ever found upon close inspection of the animals during and after anesthesia. Heart rate, as well as respiratory frequency and depth remained regular, and no changes in skin color and visible mucous membranes

Table 1 Fluorescein diacetate/propidium iodide (FDA/PI) toxicity assay results. Chinese Hamster Ovary (CHO-K1) cells (1 ml of a 2×10^5 cells/ml suspension) were incubated in the presence of the dye formula or the vehicle alone, and were subsequently stained with FDA (stains viable cells) or PI (stains dead cells) to assess their viability. 2×10^4 cells were evaluated by flow cytometry to represent each experimental condition.

	Propidium iodide		Fluorescein diacetate	
	Live (%)	Dead (%)	Live (%)	Dead (%)
Control culture	96.85	**3.15**	**95.63**	4.37
Vehicle (50 μl)	95.98	**4.02**	**94.55**	5.45
Vehicle (100 μl)	97.44	**2.56**	**97.08**	2.92
Dye formula (50 μl)	97.72	**2.28**	**95.42**	4.58
Dye formula (100 μl)	96.9	**3.1**	**94.18**	5.82

were seen. Dye-injected animals regained consciousness normally and afterward showed normal home cage activity (locomotion, eating/drinking, climbing, and grooming). Based on these observations and the *in vitro* cytotoxicity data, we can conclude that the potential *in vivo* acute toxicity of the dye is of minor significance.

3.3 *IR-676-Doped Micelles Selectively Accumulate in Areas Affected by Chemically Induced Contact Dermatitis in Mouse Ear*

Immediately 10 min postinjection, the contrast agent yielded a more than 260% greater signal in the inflamed ears than on the contralateral noninflamed side. Moreover, the signal strength showed minimal variations in the vehicle-treated ears, demonstrating the importance of body weight-based dosage. In the following 3 h, the signal strength slowly decreased in the control ears indicating the gradual clearance of the dye-loaded micelles from the circulation. At 3 h, the fluorescence intensity in the affected ears was more than 650% higher than in the controls, pointing out the prolonged presence of the extravasated dye molecules in diseased tissues [Figs. 2(a) and (b)]. The confocal fluorescence microscopic examination supported these findings, showing a patchy accumulation of the fluorophore in the perivascular regions within oxazolone-treated ears [Fig. 2(c)].

3.4 *Imaging of Deep-Tissue Inflammation of the Mouse Airways*

The 3-D tomographic imaging of the LPS-treated mice 3 h postinjection demonstrated considerably greater signal strength in the areas corresponding to the airways. Whereas in the thoracic area of PBS-treated control mice, the calculated amount of

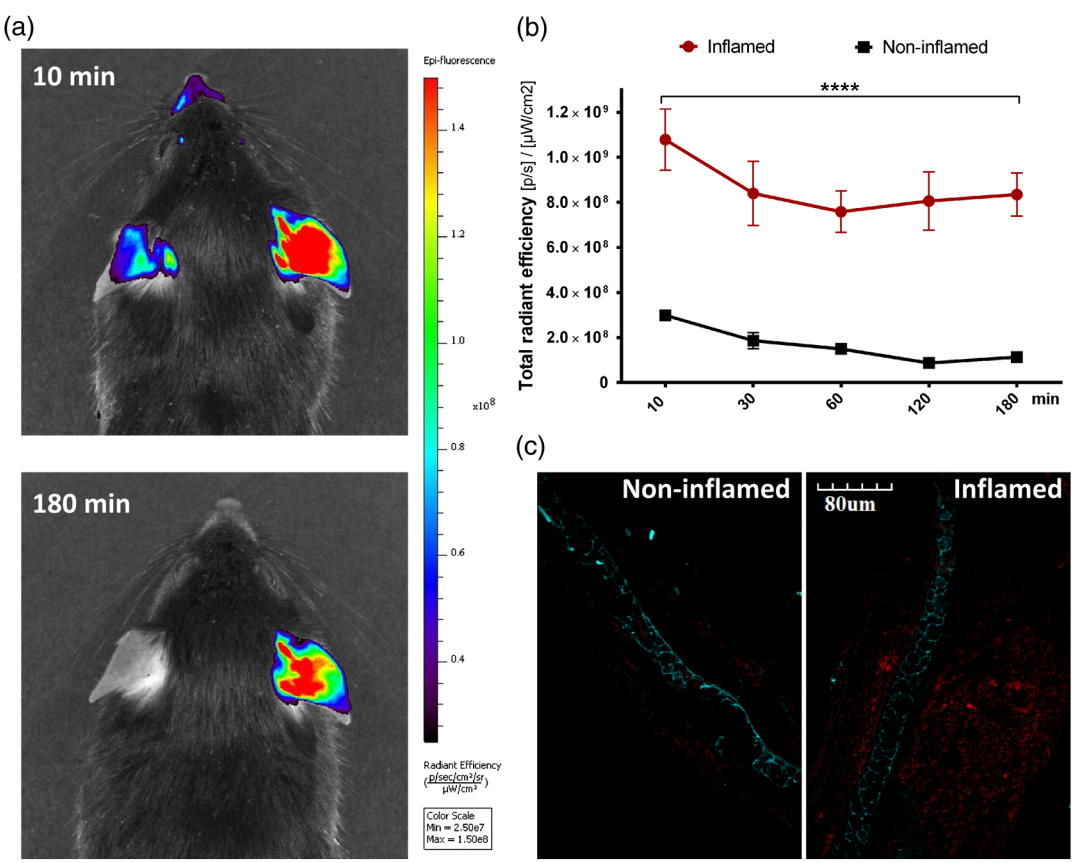

Fig. 2 Oxazolone-induced acute dermatitis on the mouse ear. (a) Representative *in vivo* epifluorescence images taken 10 and 180 min following intravenous injection of the formula. (b) The changes of fluorescence intensity in the 96% ethanol-treated control and oxazolone-treated inflamed ears throughout the measurement ($n = 7$, ****$p < 0.0001$). (c) Representative confocal fluorescence microscopy images of the control and inflamed ears harvested 3 h postinjection clearly demonstrating the tissue localization of the dye (Note: the autofluorescence of the ear cartilage is shown to provide visual aid).

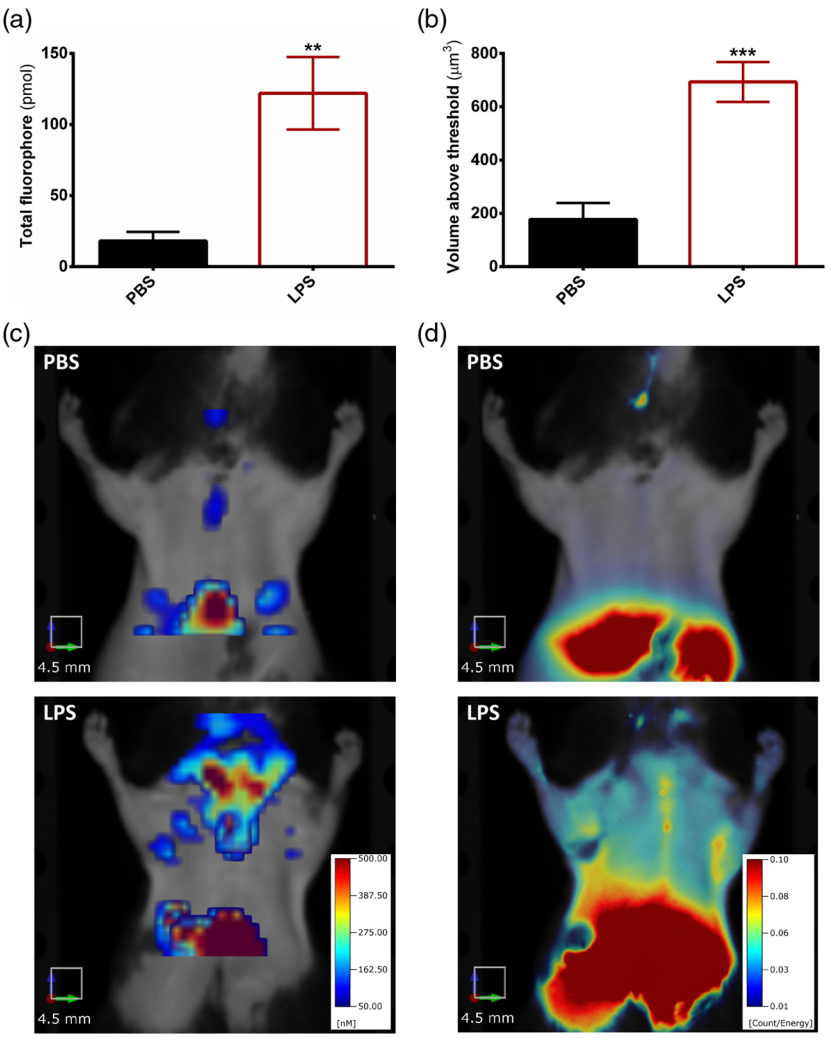

Fig. 3 Endotoxin-induced acute airway inflammation of the mouse. (a) The measured total amount of fluorophore (pmol) in the thoracic region 24 h following LPS- or PBS-challenge, 3 h after the injection of the probe. (b) The tissue volume (μm^3) affected by increased dye-accumulation. (c) Representative three-dimensional (3-D) fluorescence tomographic reconstructions. (d) Conventional epifluorescence images of the same mice for comparison. ($n = 6$/group, $^{**}p < 0.01$, $^{***}p < 0.001$).

IR-676 was only 15 to 20 pmol, LPS-treated mice displayed a 120 to 130 pmol signal strength in the respective regions [Figs. 3(a) and 3(c)]. Additionally, the area of increased plasma extravasation was significantly greater in LPS-treated mice than in the controls (on average 700 versus 200 μm^3) demonstrating that a diffuse region was affected by the LPS-induced pulmonary inflammation [Figs. 3(b) and 4]. IR-676 showed a strong accumulation in the liver, similarly to other cyanine dyes. This, however, could be easily demarcated from the specific signal (despite being at least a magnitude greater) in the 3-D tomographic scans. In contrast, it was not possible to separate the specific signal from the liver signal in the 2-D epifluorescence scans [Fig. 3(d)] due to the scattering of the latter.

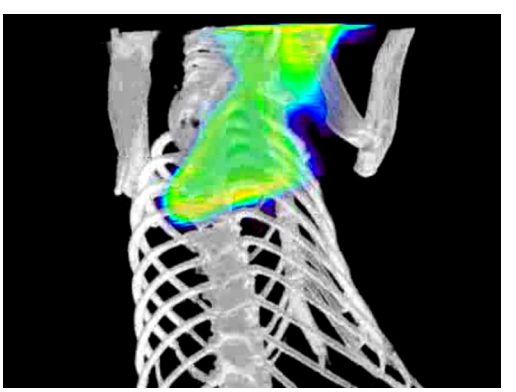

Fig. 4 Microcomputer tomography-fluorescence tomography co-registration of an LPS-treated mouse. The animal was immediately transferred upon completion of the FMT-scan into the micro-CT (Skyscan 1176, Bruker, Kontich, Belgium) remaining within the imaging cassette, where a CT-imaging of the respective region was performed. The scans were individually reconstructed, and were merged together using the AMIDE software based on three-dimensional fiducial markers present on the imaging cassette. (Video 1, MPEG, 0.92 MB) [URL: http://dx.doi.org/10.1117/1.JBO.20.1.016022.1].

3.5 *Visualization of Immune-Mediated Polyarthritis of the Mouse Ankle Joints*

In the control mice, the fluorescence in the hindlimbs was negligible 3 h after the injection (less than 1 pmol or not quantifiable) and was not localized in the ankle joints. In comparison, the K/BxN serum-treated mice displayed a circumscribed,

increased signal accumulation (~12 pmol on average) corresponding to the region of the tibiotarsal joints (affected principally by the disease), in sharp contrast to their controls [Figs. 5(a) to 5(c) and 6]. Conventional 2-D-scans of the same set of mice yielded similar results [Figs. 5(b) to 5(d)].

3.6 *Imaging Acute Carrageenan-Induced Paw Edema in the Rat*

The accumulation of signal in the treated hindpaws of the rats was clearly visible both 1 and 2 h postinjection, the signal strength being 50% and 80% greater than in the sham-treated control paws. The observed lower contrast is potentially caused by the circumscribed, local inflammation around the site of carrageenan-injection which leaves most of the paw unaffected. Thus, only a small part of the paw becomes actually inflamed, causing a comparatively modest signal surplus over the non-specific ambient background [Figs. 7(a) and 7(b)].

4 Discussion

The primary outcome of our study is that we successfully compounded a novel IR-676 dye-containing NIR imaging formula for both *in* and *ex vivo* imaging. It can be rapidly and economically established and easily mass produced for routine experimental applications using only the standard equipment and common reagents of a life sciences laboratory, with the sole exception of the fluorophore. We have validated the adaptability of our contrast agent in a range of different inflammation models in distinct organs displaying different characteristics regarding the underlying pathophysiological changes, and it proved to be a highly sensitive and perfectly reproducible tool to detect vascular leakage in mouse ear, joint and lung, as well as the rat paw.

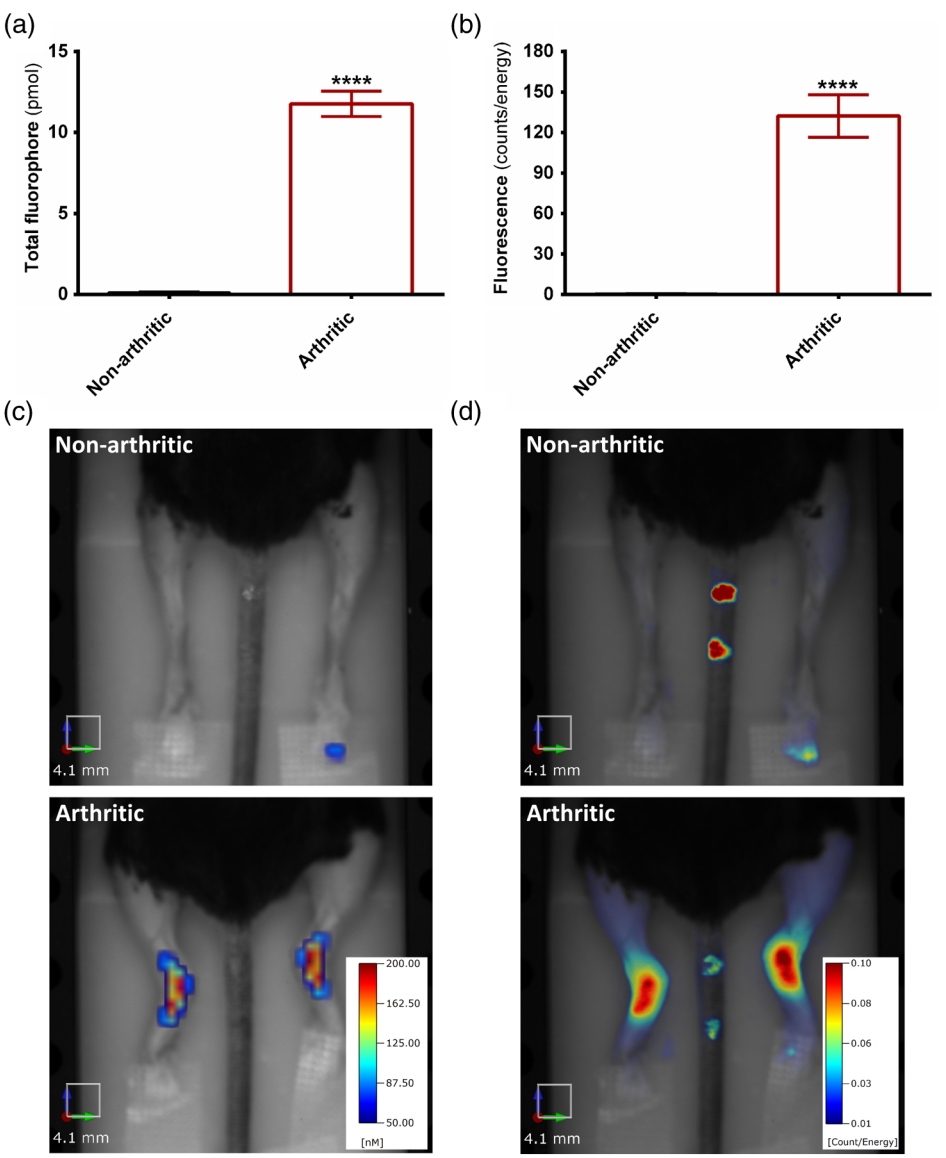

Fig. 5 K/BxN serum-induced chronic polyarthritis of the mouse. (a) The total amount of fluorophore in the ankle joints of intact and K/BxN serum-treated mice, 7 days after disease induction and 3 h following the probe injection. (b) Fluorescence intensity calculated on the basis of the conventional epifluorescence scans in the same joints. (c) Representative three-dimensional representations and (d) epifluorescence images of the same mice (Note: the numbering of the tail by a permanent marker created artifacts on the 2-D-scans). ($n = 6 - 7$/group, ****$p < 0.0001$.).

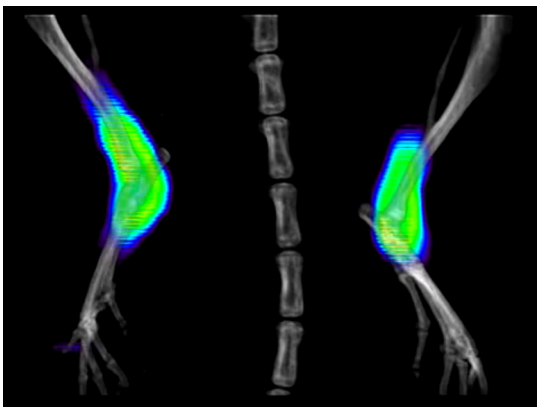

Fig. 6 Micro-CT-fluorescence tomography coregistration of an arthritic mouse. (Video 2, MPEG, 0.92 MB) [URL: http://dx.doi.org/10.1117/1.JBO.20.1.016022.2].

The observed superior contrast and signal-to-noise ratio can be attributed to several different factors: (1) employing a hydrophobic dye ensures complete encapsulation of the fluorophore and makes the amount of free dye in the aqueous phase negligible. This results in easier preparation (since it is not neccessary to test the encapsulation-efficiency); moreover, it reduces the unspecific signal from healthy tissues, which is produced at least partially by the free dye. (2) Rigorous observance of body weight-based dosage. According to our results, this alone can greatly enhance specificity mainly by reducing the variation of signal strength in controls (as observed, e.g., in the oxazolone-experiment). However, fluctuation within the diseased groups will nevertheless be present due to the intrinsic biological variations of the models.

Fluorophores encapsulated into self-assembling, microparticles using biologically inert surfactants represent a simple, yet sensitive method to evaluate a wide variety of inflammatory diseases and to follow tumor progression *in vivo*. A similar concept has recently been described for two-photon imaging microscopy using a di-stryl benzene derivative.[35] Kolliphor HS 15 and other nontoxic nonionic surfactants (Pluronic, Cremophor etc.) have been validated for the encapsulation of ICG within self-assembling micelles and provide a good solution to countervent the rapid clearance of the dye.[25,36] Nevertheless, some intrinsic problems of ICG still remain: its low quantum yield (necessitating at least a magnitude higher doses), its tendency to autoaggregate, and its broad excitation and emission maxima, making specific filtering of its fluorescence difficult. Additionally, its good water solubility poses the risk of high unspecific signal due to the unpredictable kinetics and biodistribution of the free dye. IR-676, in contrast, has a quantum yield comparable to most other advanced fluorophores (lower amounts are needed for sensitive detection),[24] and has definitive peak excitation and emission maxima, which match the parameters of the current NIR lasers and filters, as these are almost identical to the respective parameters of the most widely used NIR dyes (Cy5.5, Alexa Fluor 680 etc.). Moreover, the poor water solubility of IR-676 minimizes the presence of freely dissolved dye in the solution. We observed that IR-676 displays a robust liver accumulation, therefore, imaging disease conditions within the liver or in its close proximity are not technically possible with the present formula. We have to emphasize, however, that this is a common feature of all the other cyanine fluorophores, as well.[4,19] Additionally, it is important to note that the emission maximum of this dye lies very close to that of chlorophyll (680 to 740 nm) which is abundantly present in most standard rodent food pellets. Therefore, for imaging in the abdominal region mice should be previously fed with alfalfa-free food to reduce abdominal autofluorescence.[37] Traditionally, good water solubility was deemed as one of the essential pharmacological characteristics of fluorophores employed in *in vivo* imaging.[11] While this is generally beneficial for fluorophores intended to be used for labeling, moderate hydrophobicity increases the efficiency of micellar encapsulation and reduces unspecific background fluorescence. However, it is also important to keep in mind that lipophilic substances can have an unspecific cytotoxic effect by influencing the plasma membrane fluidity.[38] However, our *in vitro* toxicity screening test suggests that the present formula is relatively inert within its operational range, as we observed no toxic effects on CHO-K1 cells. As IR-676 is (1) not entirely hydrophobic, (2) as it was coated by the surfactant, and (3) as the employed dosage was very low compared to other similar studies, its possible *in vivo* effect (if present) was marginal at best, and caused no observable behavioral or physiologic alterations in the animals similarly to other closely related cyanine dyes.[13]

As a conclusion, the novel *in vivo* imaging formula presented here provides excellent sensitivity and high specificity in a wide range of disease models, both in superficial and deep-tissues, and it can be more easily and economically prepared using

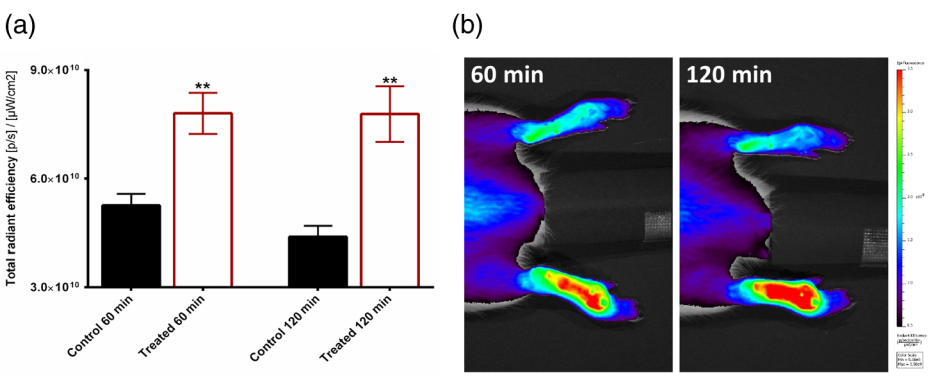

Fig. 7 Carrageenan-induced acute paw inflammation in the rat. (a) Fluorescence intensity in the saline and carrageenan-treated hindpaw (IV injection performed 2 h after disease induction), measured by epi-fluorescence imaging 60 and 120 min postinjection. (b) Representative images of the vehicle (right) and carrageenan-treated (left) hindlimbs (Note: the tail was covered to prevent possible interference caused by the concentrated dye present on the site of the IV injection). ($n = 4$, $^{**}p < 0.01$)

standard laboratory equipment without any complicated steps in the process as compared to the existing state-of-the-art NIR plasma extravasation contrast agents. Additionally, this formula can be seamlessly incorporated into most optical imaging instruments, even the fluorescent optical tomography system. IR-676-doped micelles present an excellent opportunity for the non-invasive optical imaging of plasma extravasation, and also make *in vivo* imaging of these disease conditions in larger species realistically feasible (as demonstrated on rats) due to the easy and economical large-scale synthesis of the formula.

Acknowledgments

The research was supported by the following grants: SROP-4.2.2.A-11/1/KONV-2012-0024, KTIA_NAP_13-2014-0022 (MTA-PTE NAP B Pain Research Group, identification number: 888819 to Z. Helyes), GVOP-3.2.1-2004-04-0172/3.0 and PTE ÁOK-KA-2013/24 (G. Sétáló Jr.). This work was also supported by the European Research Council—Belgium (Starting Independent Investigator Award No. 206283 to A. Mócsai), and the Wellcome Trust—United Kingdom (International Senior Research Fellowship No. 087782 to A. Mócsai). We thank Anikó Perkecz and Nikolett Szentes for their expert technical assistance, Tamás Kiss for the assistance with the micro-CT imaging, and Diane Mathis and Christophe Benoist for the KRN transgene-positive mice.

References

1. E. M. Sevick-Muraca, J. P. Houston, and M. Gurfinkel, "Fluorescence-enhanced, near infrared diagnostic imaging with contrast agents," *Curr. Opin. Chem. Biol.* **6**(5), 642–650 (2002).
2. E. Kenne and L. Lindbom, "Imaging inflammatory plasma leakage in vivo," *Thromb Haemost.* **105**(5), 783–789 (2011).
3. J. A. Nagy et al., "Vascular permeability, vascular hyperpermeability and angiogenesis," *Angiogenesis* **11**(2), 109–119 (2008).
4. K. O. Vasquez, C. Casavant, and J. D. Peterson, "Quantitative whole body biodistribution of fluorescent-labeled agents by non-invasive tomographic imaging," *PLoS One* **6**(6), e20594 (2011).
5. H. Jaffer, I. M. Adjei, and V. Labhasetwar, "Optical imaging to map blood-brain barrier leakage," *Sci. Rep.* **3**, 3117 (2013).
6. J. Saif et al., "Combination of injectable multiple growth factor-releasing scaffolds and cell therapy as an advanced modality to enhance tissue neovascularization," *Arterioscler Thromb Vasc. Biol.* **30**(10), 1897–1904 (2010).
7. A. Hansch et al., "In vivo imaging of experimental arthritis with near-infrared fluorescence," *Arthritis Rheum.* **50**(3), 961–967 (2004).
8. A. Abulrob et al., "Dynamic analysis of the blood-brain barrier disruption in experimental stroke using time domain in vivo fluorescence imaging," *Mol. Imaging* **7**(6), 248–262 (2008).
9. S. I. Prajapati et al., "Near-infrared imaging of injured tissue in living subjects using IR-820," *Mol. Imaging* **8**(1), 45–54 (2009).
10. R. Meier et al., "Indocyanine green-enhanced imaging of antigen-induced arthritis with an integrated optical imaging/radiography system," *Arthritis Rheum.* **62**(8), 2322–2327 (2010).
11. J. Pauli et al., "Novel fluorophores as building blocks for optical probes for in vivo near infrared fluorescence (NIRF) imaging," *J. Fluoresc.* **20**(3), 681–693 (2010).
12. H. Ikagawa et al., "Chemical toxicity of indocyanine green damages retinal pigment epithelium," *Invest. Ophthalmol. Vis. Sci.* **46**(7), 2531–2539 (2005).
13. R. Alford et al., "Toxicity of organic fluorophores used in molecular imaging: literature review," *Mol. Imaging* **8**(6), 341–354 (2009).
14. B. Ebert et al., "Cyanine dyes as contrast agents for near-infrared imaging in vivo: acute tolerance, pharmacokinetics, and fluorescence imaging," *J. Biomed. Opt.* **16**(6), 066003 (2011).
15. J. Klohs et al., "Near-infrared fluorescence imaging with fluorescently labeled albumin: a novel method for non-invasive optical imaging of blood-brain barrier impairment after focal cerebral ischemia in mice," *J. Neurosci. Methods* **180**(1), 126–32 (2009).
16. M. H. Kim, F. R. Curry, and S. I. Simon, "Dynamics of neutrophil extravasation and vascular permeability are uncoupled during aseptic cutaneous wounding," *Am. J. Physiol. Cell Physiol.* **296**(4), C848–C856 (2009).
17. K. Vandoorne, Y. Addadi, and M. Neeman, "Visualizing vascular permeability and lymphatic drainage using labeled serum albumin," *Angiogenesis* **13**(2), 75–85 (2010).
18. G. Egawa et al., "Intravital analysis of vascular permeability in mice using two-photon microscopy," *Sci. Rep.* **3**, 1932 (2013).
19. M. A. Yaseen et al., "Biodistribution of encapsulated indocyanine green in healthy mice," *Mol. Pharm.* **6**(5), 1321–1332 (2009).
20. B. S. Sandanaraj et al., "Fluorescent nanoprobes as a biomarker for increased vascular permeability: implications in diagnosis and treatment of cancer and inflammation," *Bioconjug. Chem.* **21**(1), 93–101 (2010).
21. X. Qi et al., "Saposin C coupled lipid nanovesicles specifically target arthritic mouse joints for optical imaging of disease severity," *PLoS One* **7**(3), e33966 (2012).
22. F. Ruchatz and H. Schuch, "Physicochemical properties of Solutol HS 15 and its solubisates," *BASF ExAct* **1**, 6–7 (1998).
23. J. Baeten et al., "Development of fluorescent materials for diffuse fluorescence tomography standards and phantoms," *Opt. Express* **15**(14), 8681–8694 (2007).
24. G. Chapman, M. Henary, and G. Patonay, "The effect of varying short-chain alkyl substitution on the molar absorptivity and quantum yield of cyanine dyes," *Anal. Chem. Insights* **6**, 29–36 (2011).
25. A. K. Kirchherr, A. Briel, and K. Mäder, "Stabilization of indocyanine green by encapsulation within micellar systems," *Mol. Pharm.* **6**(2), 480–491 (2009).
26. B. Botz et al., "Differential regulatory role of pituitary adenylate-cyclase activating polypeptide in the serum-transfer-induced arthritis model," *Arthritis Rheumatol.* **66**(10), 2739–2750 (2014).
27. F. M. Hamann et al., "Controlled modulation of serum protein binding and biodistribution of asymmetric cyanine dyes by variation of the number of sulfonate groups," *Mol. Imaging* **10**(4), 258–269 (2011).
28. K. H. Jones and J. A. Senft, "An improved method to determine cell viability by simultaneous staining with fluorescein diacetate-propidium iodide," *J. Histochem. Cytochem.* **33**(1), 77–79 (1985).
29. A. Bánvölgyi et al., "Evidence for a novel protective role of the vanilloid TRPV1 receptor in a cutaneous contact allergic dermatitis model," *J. Neuroimmunol.* **169**(1-2), 86–96 (2005).
30. S. T. Proulx et al., "Non-invasive dynamic near-infrared imaging and quantification of vascular leakage in vivo," *Angiogenesis* **16**(3), 525–540 (2013).
31. Z. Helyes et al., "Involvement of preprotachykinin A gene-encoded peptides and the neurokinin 1 receptor in endotoxin-induced murine airway inflammation," *Neuropeptides* **44**(5), 399–406 (2010).
32. B. V. Patel, M. R. Wilson, and M. Takata, "Resolution of acute lung injury and inflammation: a translational mouse model," *Eur. Respir. J.* **39**(5), 1162–1170 (2012).
33. Z. Jakus et al., "Critical role of phospholipase Cgamma2 in integrin and Fc receptor-mediated neutrophil functions and the effector phase of autoimmune arthritis," *J. Exp. Med.* **206**(3), 577–593 (2009).
34. J. C. Fehrenbacher, M. R. Vasko, and D. B. Duarte, "Models of inflammation: carrageenan- or complete Freund's adjuvant (CFA)-induced edema and hypersensitivity in the rat," *Curr. Protoc. Pharmacol.* **56**(5), 4:5.4.1–5.4.4. (2012).
35. M. Maurin et al., "Deep in vivo two-photon imaging of blood vessels with a new dye encapsulated in pluronic nanomicelles," *J. Biomed. Opt.* **16**(3), 036001 (2011).
36. T. H. Kim et al., "Evaluation of temperature-sensitive, indocyanine green-encapsulating micelles for noninvasive near-infrared tumor imaging," *Pharm. Res.* **27**(9), 1900–1913 (2010).
37. Y. Inoue et al., "Diet and abdominal autofluorescence detected by in vivo fluorescence imaging of living mice," *Mol. Imaging* **7**(1), 21–27 (2008).
38. I. Cascorbi and M. M. Forêt, "Interaction of xenobiotics on the glucose-transport system and the Na + /K(+)-ATPase of human skin fibroblasts," *Ecotoxicol. Environ. Saf.* **21**(1), 38–46 (1991).

Biographies of the authors are not available.